ACS NANO
Cite This: ACS Nano 2018, 12, 9587−9595
www.acsnano.org
ARTICLE

Trichogenic Photostimulation Using Monolithic Flexible Vertical AlGaInP Light-Emitting Diodes

Han Eol Lee,[†,¶] Seung Hyun Lee,[†,¶] Minju Jeong,[‡] Jung Ho Shin,[†] Yuri Ahn,[§] Daesoo Kim,[‡] Sang Ho Oh,[§] Seok Hyun Yun,[∥] and Keon Jae Lee[*,†]

[†]Department of Materials Science and Engineering, Korea Advanced Institute of Science and Technology (KAIST), 291 Daehak-ro, Yuseong-gu, Daejeon 34141, Republic of Korea

[‡]Department of Biological Sciences, Korea Advanced Institute of Science and Technology (KAIST), 291 Daehak-ro, Yuseong-gu, Daejeon 34141, Republic of Korea

[§]Department of Dermatology and Cutaneous Biology Research Institute, Severance Hospital Yonsei University College of Medicine, 50-1 Yonsei-ro, Seodaemun-gu, Seoul 03722, Republic of Korea

[∥]Wellman Center for Photomedicine, Harvard Medical School and Massachusetts General Hospital, 65 Landsdowne Street Up-5, Cambridge, Massachusetts 02139, United States

Supporting Information

ABSTRACT: **Alopecia is considered an aesthetic, psychological, and social issue among modern people. Although laser-induced skin stimulation is utilized for depilation treatment, such treatment has significant drawbacks of high energy consumption, huge equipment size, and limited usage in daily life. Here, we present a wearable photostimulator for hair-growth applications using high-performance flexible red vertical light-emitting diodes (f-VLEDs). Flexible microscale LEDs were effectively fabricated by a simple monolithic fabrication process, resulting in high light output (∼30 mW mm^{-2}), low forward voltage (∼2.8 V), and excellent flexibility for wearable biostimulation. Finally, trichogenic stimulation of a hairless mouse was achieved using high-performance red f-VLEDs with high thermal stability, device uniformity, and mechanical durability.**

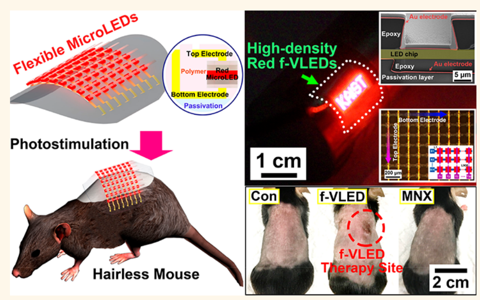

KEYWORDS: *microLED, flexible vertical LED, red LED, bioelectronics, phototherapy, hair growth*

Numerous people around the world have suffered from alopecia, which leads to aesthetic issues, low self-esteem, and social anxiety.[1,2] With the population expansion of alopecia patients from middle-age down even to the twenties, a depilation treatment is expected to have social and medical impacts on billions of patients.[3] The causes of alopecia are generally known to be heredity,[4] mental stress,[5] aging,[6] and elevated male hormone.[7−9]

Therapeutic techniques such as thermal,[10] electrical,[11] pharmacological,[12] and optical stimulation[13,14] have been proposed to treat hair problems. Among them, laser stimulation to hair-loss regions is a promising technique, activating the anagen phase and the proliferation of hair follicles without side effects.[14−18] In particular, periodic irradiation with a red light with wavelength of 650 nm on the hairless area can assist localized stimulation of hair follicles under the skin, because these waves can deeply penetrate the skin tissue, compared to the short wavelengths of blue and green light.[19−23] However, this laser stimulation technique has drawbacks, such as high power consumption, large size, and restrictive use in daily life (e.g., the difficulty of microscale spatial control and the long time exposure of high-energy laser).[24−27]

Recently, flexible inorganic-based micro-light-emitting diodes (μLEDs) have been spotlighted for future display and biomedical devices,[28−33] such as biosensors, pulse oximetry (SpO_2) sensors, and optogenetic stimulators. These flexible μLEDs are suitable for human-interface applications, due to their biocompatibility, portability, and excellent stability. However, flexible μLEDs still have critical challenges in application to wearable phototherapeutic devices, including high heat radiation, low optical efficiency, and high energy consumption.[28,34−38] Our group has demonstrated flexible thin-film vertical μLEDs (f-VLEDs) with both blue and red light with high stability and outstanding power efficiency.[39−41]

Received: July 24, 2018
Accepted: August 20, 2018
Published: August 20, 2018

DOI: 10.1021/acsnano.8b05568
ACS Nano 2018, 12, 9587−9595

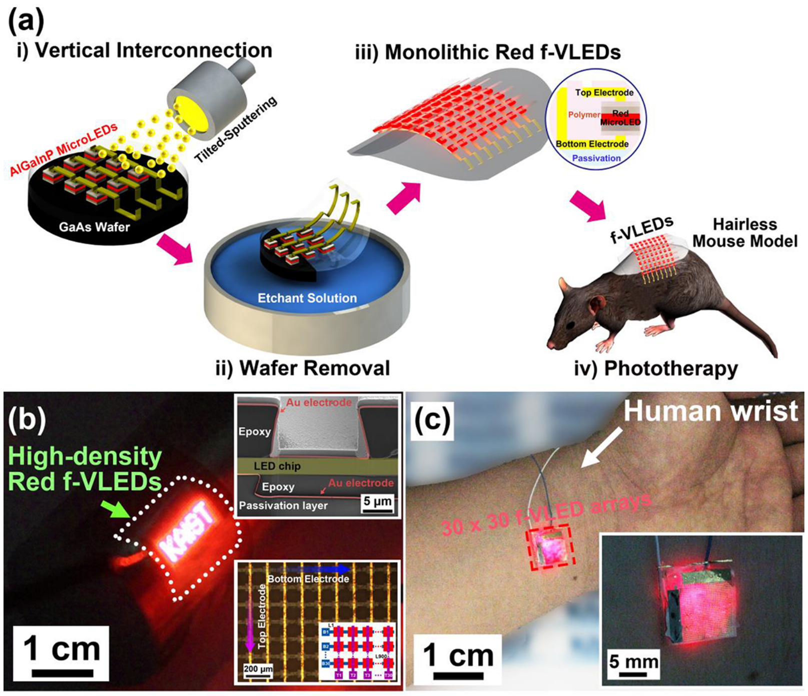

Figure 1. (a) Schematic illustration of the fabrication procedure and trichogenic photostimulation by monolithic flexible AlGaInP vertical LEDs. (b) Optical image of monolithic f-VLED with red word "KAIST" under bending state. The upper inset is a cross-sectional SEM image of monolithic red f-VLED. The lower inset image exhibits a magnified microscopic image of 30 × 30 f-VLEDs with a 50 × 50 μm^2 chip. (c) Photograph of red f-VLED array affixed on surface of human wrist. The inset is a magnified picture of the 30 × 30 LED array.

Despite the excellent properties of these devices, the biomedical and thermal effects of f-VLEDs were not investigated on living animals, which were significant to wearable and phototherapeutic applications. In addition, a phototherapeutic investigation for alopecia treatment should be additionally required for clinical applications.

Herein, we report high-performance 30 × 30 AlGaInP f-VLEDs enabled by transfer-free monolithic fabrication for a wearable trichogenic photostimulator. Ultrathin flexible μLEDs with 3 μm thick active layers were fabricated with simple monolithic vertical interconnection of top n- and bottom p-electrodes. The red f-VLED arrays were conformally attached on a human wrist with high irradiance of ~30 mW mm^{-2} and low forward voltage of ~2.8 V. The red light with long wavelength of 650 nm enabled to deeply penetrate the skin and stimulate the hair follicles, located 2 mm under the dermal surface. The thermal stability of the monolithic f-VLED was theoretically investigated using finite element method (FEM) simulation and experimentally optimized using sophisticated photothermal modulation for wearable skin stimulation. Our monolithic f-VLEDs exhibited excellent mechanical reliability during harsh periodic bending/unbending motions, which is beneficial for skin-attachable phototherapies. Finally, trichogenic photostimulation was performed to incite hair growth in a living depilated mouse via low-heating f-VLED array, based on the previous clinical research.[42,43] We verified hair regrowth in the mice and analyzed immunofluorescent and histological effects to confirm the phototherapy applications of our f-VLEDs.

RESULTS AND DISCUSSION

Monolithic Red f-VLEDs for Phototherapy. Figure 1a schematically illustrates the device fabrication and trichogenic stimulation of a hairless mouse using monolithic red f-VLEDs. The monolithic f-VLED fabrication process is as follows: (i) High-purity AlGaInP LED layers were grown by metal–organic chemical vapor deposition (MOCVD) on a rigid GaAs wafer. The μLED chips with p-ohmic contacts (Cr/Au) were made on the GaAs substrate and isolated using an epoxy-based photoresist with 10 μm thickness. The polymeric isolation layer had two contact holes, which were p-electrode contacts and vertical passageways from bottom to top surface. The metallic p-electrodes were deposited by tilted radio frequency (RF) sputtering and patterned by a conventional photolithography process on the isolation layer. (ii) The biocompatible polymer covered the top surface of the device, as a passivation layer of the f-VLED. The passivated LED device was flipped-over, and then the mother GaAs wafer was selectively removed by a solution of hydrogen peroxide (H_2O_2, 13 wt %) and citric acid ($C_6H_8O_7$, 30 wt %) at 50 °C. (iii) Au metal electrodes were formed on the flipped LEDs as top n-electrodes and bottom p-electrode pads. (iv) To optically stimulate the shaved region of mouse skin, the wearable red f-VLED array was conformally attached on the mouse dorsal surface (see Figure S1 in the Supporting Information for the detailed device fabrication processes). Figure 1b shows high-density monolithic f-VLEDs on a round metal bar (bending curvature radius of 5 mm), successfully presenting the word "KAIST". The vertically interconnected f-VLED array was composed of 900 μLEDs in the passive-matrix (PM) with 50 × 50 μm^2-sized LED chips, as shown in the lower inset of Figure 1b. Using a transfer-free monolithic process, microscale LED chips were constructed on a flexible polymer matrix with high production yield (over 95%). Simultaneously, the thickness of the entire f-VLED device was reduced to 20 μm including polymer substrates, which was ~60% thinner than that of our previous reported f-VLEDs.[32] As shown in the upper inset of Figure 1b, a cross-sectional scanning electron microscopy

DOI: 10.1021/acsnano.8b05568
ACS Nano 2018, 12, 9587−9595

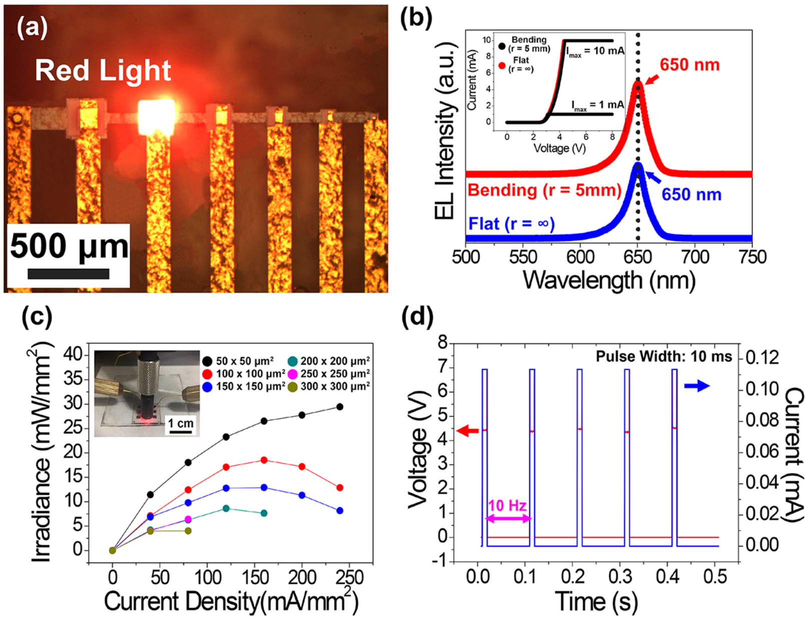

Figure 2. (a) Magnified optical image of monolithic red f-VLEDs composed of 6 different-sized LED chips (300 × 300 μm^2, 250 × 250 μm^2, 200 × 200 μm^2, 150 × 150 μm^2, 100 × 100 μm^2, and 50 × 50 μm^2). (b) Electroluminescence spectrum of red f-VLED (wavelength of 650 nm) under flat and bent states (bending radius of 5 mm). The inset is I−V graphs of the red f-VLED. (c) Optical output density of various-scale LEDs as a function of current density. The inset shows a picture of red LED during irradiance measurement. (d) Pulsed-operation graph of monolithic red f-VLED (frequency of 10 Hz).

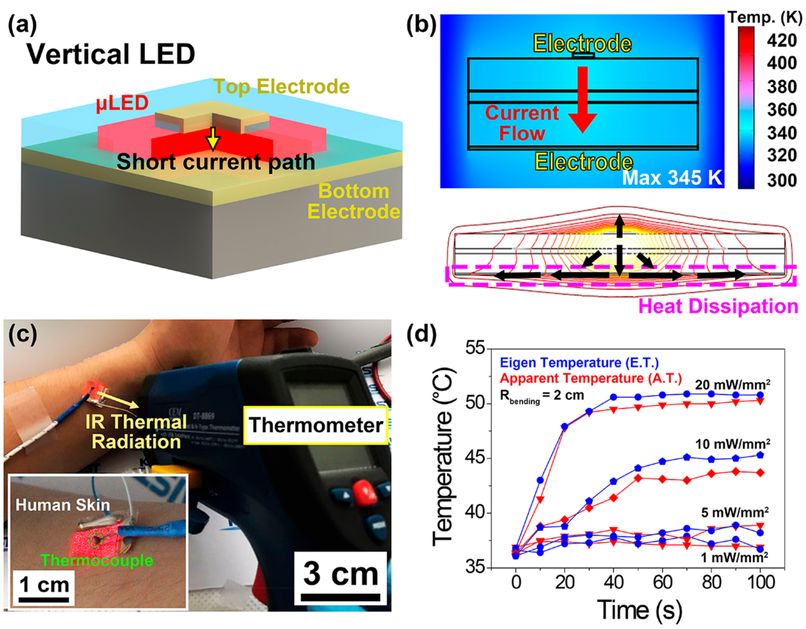

Figure 3. (a) 3D schematic illustrations of flexible vertical-structured LED (f-VLED) with short current path. (b) Heat distribution by FEM calculation when current of 10 mA is applied to f-VLED (top). Isothermal image of f-VLED during light emission (bottom). (c) Photograph of temperature analysis in monolithic f-VLEDs on human wrist. Thermometer measures the actual temperature and apparent temperature using a thermocouple and IR thermal radiation, respectively. The inset is a magnified image of the thermocouple and skin-attached f-VLEDs while detecting the actual temperature. (d) Actual measured temperature (ET) and apparent temperature (AT) of 30 × 30 monolithic f-VLEDs during light emission. ET and AT were measured on the human wrist with bending radius of 2 cm.

(SEM) image depicts the 3.5 μm-thick AlGaInP LED layers, embedded in a polymer epoxy layer of 20 μm thickness without any defects. In addition, it was possible to resolve the critical step-coverage issue of f-VLED by tilted-sputtering deposition, as demonstrated in the interconnecting metal electrodes on the sidewall and the LED top surface (marked by the red line in the upper inset of Figure 1b). The 30 × 30 ultrathin f-VLED array can be stably attached to the human wrist with biocompatible glue, as shown in Figure 1c. Despite active wrist movement, the conformally attached PM f-VLED array successfully emitted a stable red glow on the human skin without delamination or breakdown, indicating the possibility of consistent phototherapy for alopecia treatment in daily life.

DOI: 10.1021/acsnano.8b05568
ACS Nano 2018, 12, 9587−9595

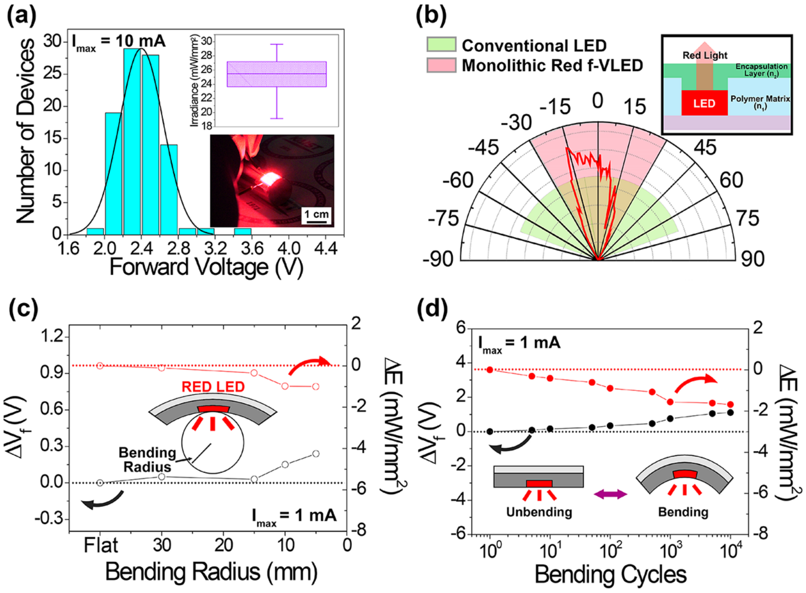

Figure 4. (a) Statistical distribution with forward voltage of 100 LEDs. The upper inset is a box-whisker graph of the optical output density. The lower inset displays a 10 × 10 red VLED array under bending condition. (b) Light extraction of monolithic red LED. The red region and the gray region indicate the emission angle of monolithic f-VLED and conventional LED, respectively. The inset image is a simple cross-sectional picture of monolithic red LED. (c) Electrical properties of f-VLEDs with various bending radius of 40, 30, 15, 10, and 5 mm (concave bending). (d) Fatigue test results of forward voltage and irradiance during 100 000 bending/unbending motions (concave bending).

Electrical and Optical Properties of f-VLEDs. For trichogenic modulation of specific skin areas, the chip size of the f-VLEDs has to be sophisticatedly tuned, based on the optical and electrical characteristics. Figure 2a presents a magnified optical image of six different sized f-VLEDs. From the left side, the LED chip sizes are 300 × 300 μm^2, 250 × 250 μm^2, 200 × 200 μm^2, 150 × 150 μm^2, 100 × 100 μm^2, and 50 × 50 μm^2, respectively. Figure 2b shows electroluminescence (EL) characteristics of a monolithic f-VLED under flat and bending conditions. The f-VLED displayed a sharp emission peak of red light with 650 nm wavelength, regardless of the flat and bent state. The CIE 1931 color coordinates of the f-VLEDs were (0.6998, 0.3014), showing the high chroma and hue of the red light, as shown in Figure S2 in the Supporting Information. Since red light with wavelength from 600 to 700 nm can penetrate deeply under the skin to approximately 2 mm, our red f-VLEDs are effective to stimulate the hair follicles, located at 1~2 mm below the skin surface.[19−21,27] The inset of Figure 2b is $I-V$ curves of the monolithic f-VLEDs, indicating a low forward voltage (V_f) of 2.8 V under flat and bent states. Figure 2c exhibits the optical output power density of the f-VLEDs for the different-sized chips. As plotted in these graphs, the output power of the f-VLEDs increased as the chip size decreased. The 50 × 50 μm^2-sized LED had a maximum light output power of 29.4 mW mm^{-2} at 1 mA, which was 200% higher than that of the 100 × 100 μm^2-sized optical device. This high irradiance of the small-sized μLED was attributed to the low junction temperature during light emission, due to its low internal resistance.[32,44−46] We chose this 50 × 50 μm^2-sized red f-VLED for skin-attachable phototherapy applications due to its deep light penetrability and low power consumption (50 mW for a irradiance of 1 mW mm^{-2}) compared to the conventional phototherapeutic lasers (20 W for irradiance of 1 mW mm^{-2}).[47,48] Figure 2d and Figure S3 in the Supporting Information show the pulse operation of monolithic f-VLEDs at 10 and 20 Hz, which can decrease the LED heat generation during skin phototherapy compared to continuous wave (CW) light.[25,49,50] The red f-VLEDs were pulse-driven by an ~0.11 mA current at 10 ms intervals, leading to a constant voltage response (4.5 V).

Thermal Stability of f-VLEDs. Thermally stable operation of f-VLEDs is essential for application to skin-attachable devices without dermal damage, such as erythema, swelling, and low-temperature burns.[14,18,51] To investigate the thermal stability of monolithic f-VLEDs, an AlGaInP f-VLED was modeled with short 3.5 μm current path on ultrathin flexible substrates, as shown in Figure 3a. Figure 3b and S8 depict theoretical heat distribution of the monolithic f-VLED, calculated by the FEM Joule heating mode. The resistive heating of the μLED was defined by eq 1.[32]

$$Q = I^2Rt \tag{1}$$

Here, Q is the heat caused by Joule heating, I denotes the injection current, R is the device resistance, and t is the LED operation time. The generated heat in a μLED chip is conducted to the electrodes, passivation layer, and ultrathin flexible substrates. This conductive heat transfer in the f-VLED was calculated by heat transfer eq 2.

$$\text{heat}(Q) = \rho C_P \frac{\partial T}{\partial t} - \nabla(k\nabla T) \tag{2}$$

where ρ is the density of the various materials such as the electrode, n-AlGaInP, p-AlGaInP, and multiquantum well (MQW), C_P is the heat capacity, and k is the thermal conductivity. When a 10 mA current was injected into the f-VLED, the maximum temperature of the flat and bent f-VLED was estimated to 345 (Figure 3b) and 350 K (Figure S8), respectively. Despite the high injection current, the low temperature of the f-VLED came from the sub-10 μm current path of the microscale LED chip, which resulted in a low

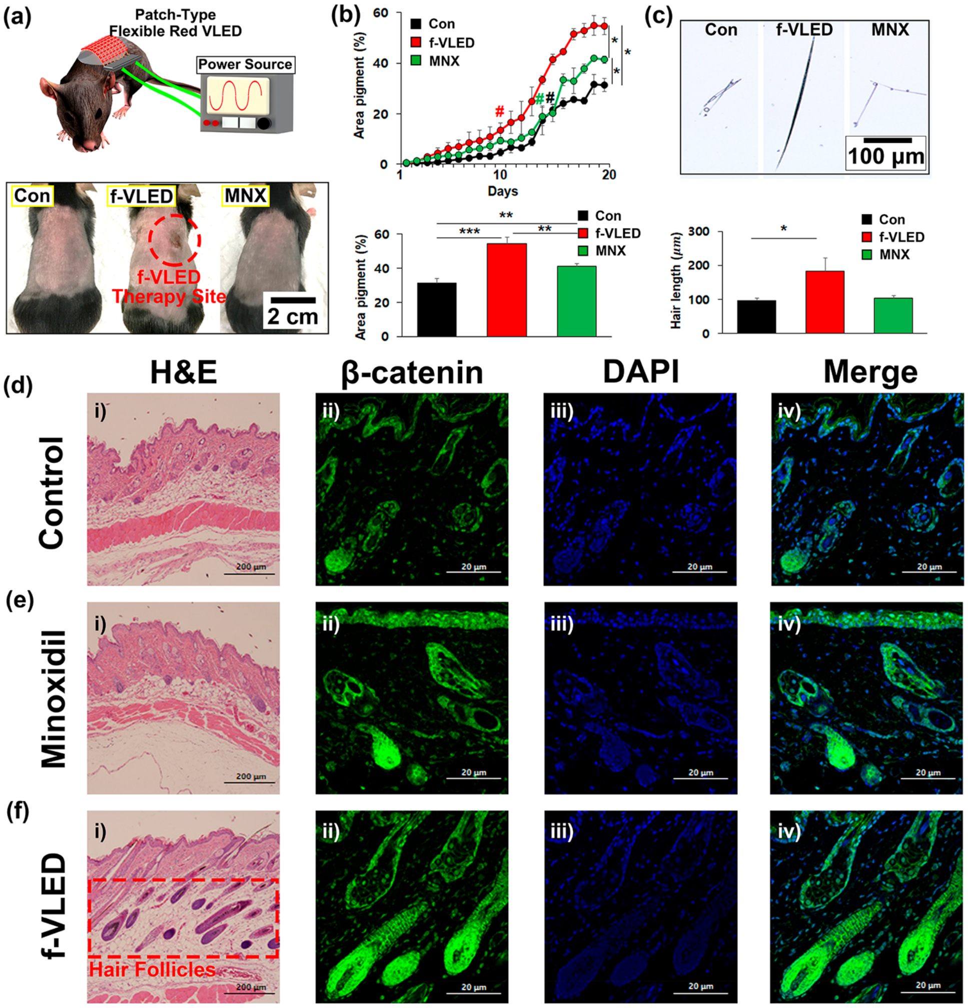

Figure 5. (a) Conceptual illustration of trichogenic photostimulation via monolithic red f-VLEDs (top). Photographs of mouse dorsal skin in control, f-VLED-treated, and MNX-treated groups (bottom) after 20 days of hair-regrowth experiments. (b) Hair-regrowth area as a function of skin stimulation days (top). Hair-regrowth experiment results of f-VLED-treated and MNX-treated mice, which were treated for 20 consecutive days (bottom) (*p < 0.05, paired t test, #p < 0.05, two way ANOVA; **p < 0.01, ***p < 0.001, paired t test). Number of mice used for analyses: light-treated, n = 4; MNX-treated, n = 4; negative control, n = 4. (c) Extracted hair images of mice after biological experiments (top) of 20 days. Comparison of hair-growth length after trichogenic treatments (bottom) (*p < 0.05, paired t test). Histological and immunofluorescence results of stimulated mouse dorsal skin in (d) control, (e) MNX, and (f) f-VLED group {(i) H&E stained images, (ii) β-catenin stained images, (iii) DAPI stained images, (iv) merged images}.

internal electrical resistance,[45,52] as depicted in Figures S10 and 11 in the Supporting Information. In-depth analysis of this phenomenon can be clarified by the isothermal mapping image in the bottom of Figure 3b and Figure S9. According to the simulation results, AlGaInP f-VLED lowered its junction temperature by utilizing the bottom electrode as a heat sink, dissipating the heat from the LED chip to the outside.[40]

To verify the thermal stability of the monolithic f-VLEDs experimentally, the f-VLED temperature was investigated on human skin by modulating the LED irradiance (Figure 3c). For accurate evaluation, the μLED temperature was analyzed by two methods of noncontact and contact measurements. The infrared (IR) radiant temperature of the LED surface, defined as the apparent temperature (AT), was detected using a noncontacting thermometer, while the conductive heat of the f-VLED, defined as the eigen temperature (ET), was measured using a contacting thermocouple, as shown in the inset of Figure 3c. Figure 3d presents temperature measurement results for f-VLEDs at different levels of light irradiance of 1, 5, 10, and 20 mW mm^{-2} on the human wrist (bending radius of 2 cm). The LED temperature depending on power density was proportional to the irradiation time and finally saturated at 51, 45, 38, and 37 °C for 20, 10, 5, and 1 mW mm^{-2}, respectively. When the skin-attached f-VLED radiates red light of 1−5 mW mm^{-2}, the skin temperature should be maintained at <40 °C without any thermal damage of the tissue.[49,53] It is noteworthy that the low-heating and thermal stability of the monolithic f-VLEDs make this device suitable for wearable phototherapeutic applications in daily life, due to its high performance without thermal skin damage.

Uniformity and Mechanical Stability of f-VLEDs. In order to confirm the uniformity of our monolithic f-VLEDs, the forward voltage (V_f) and irradiance of the 10 × 10 LEDs were measured at 10 mA operation current. As displayed in Figure 4a, the statistical bar chart of V_f presents a Gaussian distribution, showing that 91% of LEDs have V_f in the range of 2.1−2.7 V. The upper inset of Figure 4a is a box-whisker graph of f-VLED irradiance, depicting the average optical output density of 25.5 mW mm^{-2}. Figure 4b presents light distribution curves of the thin-film f-VLED, compared to the

DOI: 10.1021/acsnano.8b05568
ACS Nano 2018, 12, 9587−9595

bulky commercial LED with wide light radiation. Our f-VLED had a narrow light radiation angle of 60°, which was caused by the total internal reflection between the encapsulation layer and the polymer matrix,[54,55] as shown in the inset of Figure 4b. It was possible to achieve the total reflection of the f-VLED by optimizing the device structure and the component materials. Based on Snell's law, the top encapsulation layer was carefully selected as transparent polymer with a large refractive index of n_{el} = 1.67 compared to that of the polymer matrix (n_{pm} = 1.56). According to the mathematical calculation, the emitted light was focused and propagated with high straightness through a microhole of the polymer matrix, as shown in Figure S12. The concentrated light emission of our f-VLED indicates that monolithic f-VLEDs can locally stimulate the targeted skin area without any side effects to unintended regions. To confirm the applicability to depilation treatment, the mechanical reliability tests of f-VLEDs were fulfilled in the concave bending state, which was similar condition with wearable trichogenic treatment. The mechanical stability of the f-VLED was examined by observing the V_f change at different bending curvature radius, as shown in Figure 4c. Despite the severe bending state with curvature radius of 5 mm, V_f increased only by 0.24 V on the half-cylindrical PDMS mold. Figure 4d exhibits the outstanding mechanical reliability of the f-VLEDs at a bending radius of 5 mm. After 10 000 bending/unbending cycles, V_f increased by 1.1 V and the irradiance decreased by 1.68 mW mm^{-2}. The excellent mechanical durability is attributed to the structure and design of the monolithic f-VLED, which can freely adjust the stress-free region (SFR) of ultrathin flexible LED devices. The SFR can be expressed by the following equation.[56−58]

$$h_{\text{neutral}} = \frac{\sum_{i=1}^{n} \bar{E}_e t_i \left\{ \left(\sum_{j=1}^{i} t_j \right) - \frac{t_i}{2} \right\}}{\sum_{i=1}^{n} \bar{E}_e t_i} \tag{3}$$

where n is the number of component layers, t_i is the thickness of the ith layer, and $\bar{E}_e$ is the effective Young's modulus. According to eq 3, the SFR was located at the middle of the AlGaInP LED chip (nearly 7.8 μm above the device bottom), as shown in Figure S13 in the Supporting Information. Optimized SFR of the ultrathin f-VLED was easily realized by controlling the polymer thickness of the device through spin-coating. The mechanically stable f-VLEDs can be used in wearable patch photostimulators, because they can endure periodic mechanical stress from biomechanical motions.

Trichogenic Photostimulation of Mouse Dorsal Skin via Monolithic Red f-VLEDs. To verify the trichogenic effect of the skin-attachable f-VLEDs, the reliable evaluation of hair growth was carried out in 12 7-week-old female mice during 20 consecutive days, based on the previous clinical studies, as shown in Figure 5a.[42,43] The dorsal hair of mice was shaved off, and mice were assigned to negative control, positive control, and red f-VLED-treated groups; while mice in the positive control (n = 4) were treated daily with injections of minoxidil (MNX) solution to the intradermal region under the mouse dorsal skin (injection quantity, 30 μL of 1 μM),[16] the negative control group (n = 4) was maintained without any treatment. The shaved skin of the experimental group (n = 4) was optically stimulated by patch-type f-VLEDs at 5 mW mm^{-2} for 15 min every day. The bottom images of Figure 5a are photographs of mouse dorsal skin after 20 days of hair-regrowth experiments. Mice in the experimental group presented local hair regrowth in light-irradiated regions, while control groups exhibited negligible changes in the mouse dorsal skin. Figure 5b shows areal comparisons of hair-regrown regions after *in vivo* animal experiments. The light-treated group showed a faster hair-growth tendency than that of other groups as time went by. The percentage of hair-regrowth area was measured for confirming the trichogenic effect of f-VLED, instead of the standard microscopic hair counting.[6,59] The photostimulated mice exhibited a wider hair-regrowth area (59.76% in 1 × 1 cm^2) than those of other groups (36.16% in negative control group and 42.78% in positive control group). Figure 5c displays length comparisons of the extracted mouse hairs after 20 days of biomedical experiments. The 183.2 μm length of the photostimulated mouse hair was remarkably longer than 103.6 μm of the positive control group. Red light with a wavelength of ∼650 nm is known to accelerate the proliferation and anagen entry of hair follicle cells, which are closely related to hair re-growth.[15,21,59] In order to confirm the follicle increasing effect of monolithic f-VLEDs, histological and immunofluorescence analyses were performed on the extracted skin tissues, as shown in Figure 5d−f. After hair-regrowth experiments, the mouse dorsal tissues were cut into thin slices, and stained with hematoxylin and eosin (H&E), 4′,6-diamidino-2-phenylindole (DAPI; blue fluorescence), and β-catenin (green fluorescence). Figure 5f−i displays histological results of the photostimulated skin tissue. Mouse hair follicles proliferated more in the light-treated skin compared with the control groups, as presented in Figure 5d,e(i). The β-catenin expression was evaluated in immunofluorescence tests, since it is closely associated with Wnt signaling, which is the most important factor in hair follicle development.[60−63] As shown in Figure 5f(ii), the β-catenin protein was prominently expressed in the experimental group compared to the control groups (Figure 5d,e(ii). These results demonstrate that the red light of f-VLED successfully accelerated the Wnt/β-catenin signal, enabling the proliferation of hair follicle cells and enhancing anagen entry of mouse dorsal hair.[64]

CONCLUSIONS

In summary, we demonstrated a skin-attachable trichogenic photostimulator using high-performance AlGaInP f-VLEDs. Ultrathin 30 × 30 red f-VLEDs with high optical output of 30 mW mm^{-2} were stably attached to human skin without cracking or delamination. The 10 Hz-pulsed red light with a peak wavelength of 650 nm enabled deep dermal stimulation of the subcutaneous tissue. The excellent thermal stability of monolithic f-VLED was theoretically confirmed by Joule heating and heat flux mode of FEM simulation. In addition, the f-VLED exhibited a narrow light emission angle of 60° and superior mechanical reliability in 10 000 harsh bending fatigue tests, indicating its possibility for use in skin-attachable phototherapeutic device. Finally, our red f-VLED stimulator was readily implemented on the dorsal skin of the depilated mice, enabling hair-growth photostimulation. The hair growth of the depilated mouse was promoted by periodic irradiation of red light for 20 consecutive days. After the red f-VLEDs irradiated the mouse skin, the hair growth-related Wnt/β-catenin signal was observed in the extracted mouse skin without any thermal or inflammatory tissue damage. This approach confirms that our red f-VLEDs are powerful tools for real-time phototherapy applications, such as wound healing, acne care, and skin lightening.

DOI: 10.1021/acsnano.8b05568
ACS Nano 2018, 12, 9587−9595

EXPERIMENTAL SECTION

Electrical Measurements. *I*−*V* curves of the monolithic LEDs were analyzed using a Keithley 4200-SCS with current sweep mode. Periodic pulsed current was applied to f-VLEDs using a Keithley 2612A (frequency of 10 and 20 Hz and pulse width of 10 ms).

Optical Measurements. The optical properties of the red AlGaInP LEDs were determined by AvaSpec-UlS2048-RS optic spectroscopy (Avantes Corp.). The EL and optical output density were measured with current density from 40 to 240 mA/mm^2. The cross-sectional light emission distribution was analyzed using a GP-200 goniophotometer (Murakami Color Research Laboratory).

Bending Test. The optical/electrical characteristics of monolithic AlGaInP LEDs were measured on a half-cylinder PDMS mold with bending curvature from 5 to 30 mm.[65] The mechanical fatigue test of f-VLEDs was performed on a QS48 periodic bending motion machine (TPC motion Corp.) and a Keithley 230 power source meter.[66] Irradiance and turn-on voltage were determined after periodic deformation cycles of 10 000 cycles with 2 Hz frequency.

Animals. All animal care and experiments were performed according to the directives of the Animal Care and Use Committee of the Korea Advanced Institute of Science and Technology (KAIST, Korea). The mice were maintained under 12 h light/dark cycle (light cycle beginning at 6:00) at room temperature with *ad libitum* access to food and water.

Trichogenic Stimulation Test. Twelve female 7-week-old mice of were used to test the trichogenic effects of MNX and red f-VLEDs for consecutive 20 days. MNX (30 μL of 1 μM) was injected into the intradermal area of mice in the positive control group. MNX injection was accomplished by the intralesional injection method, which can solve the insufficient trichogenic effect of the endermic drug and reduce the side-effects of the general injection methods. The red light of the f-VLED (900 LEDs with 5 mW mm^{-2} irradiance) was used to irradiate the mouse dorsal skin in the experimental group for 15 min every day, as shown in Figures S18−20.

ASSOCIATED CONTENT

Supporting Information

The Supporting Information is available free of charge on the ACS Publications website at DOI: 10.1021/acsnano.8b05568.

> Detailed schematics of fabrication process, color coordinates and pulse operation of the f-VLEDs, 3D illustration of LLED and VLED structures, heat distribution and isothermal image of LLED, calculated temperatures for LLED and VLED, simulated temperature distribution and isothermal image of bent f-VLED, simplified structure and circuit diagram of LLED and VLED, Total reflection at the polymer interface between polymer matrix and passivation layer in the monolithic AlGaInP f-VLED, schematic explanation of mechanical neutral plane in monolithic f-VLEDs, electrical characteristics of red f-VLEDs with various bending curvature radius, mechanical fatigue test results, mechanical fatigue test results, and photographs of the trichogenic stimulation experiment set up and results (PDF)

AUTHOR INFORMATION

Corresponding Author

*E-mail: keonlee@kaist.ac.kr.

ORCID

Keon Jae Lee: 0000-0001-7500-3079

Author Contributions

¶H.E.L. and S.H.L. contributed equally to this work.

Notes

The authors declare no competing financial interest.

ACKNOWLEDGMENTS

This work was financially supported by Creative Materials Discovery Program (NRF-2016M3D1A1900035) and Global Frontier R&D Program of the Center for Integrated Smart Sensors (CISS-2016M3A6A6929958) through the National Research Foundation of Korea (NRF) funded by the Ministry of Science, ICT, and Future Planning. This work was supported by National Research Foundation (NRF) of Korea funded by the Ministry of Science, ICT, and Future Planning (Grant No. NRF-2014R1A2A1A12067558 and 2012-0008779).

REFERENCES

(1) Pratt, C. H.; King, L. E.; Messenger, A. G.; Christiano, A. M.; Sundberg, J. P. Alopecia Areata. *Nat. Rev. Dis. Prim.* **2017**, *3*, 17011.

(2) Pirastu, N.; Joshi, P. K.; De Vries, P. S.; Cornelis, M. C.; McKeigue, P. M.; Keum, N.; Franceschini, N.; Colombo, M.; Giovannucci, E. L.; Spiliopoulou, A.; Franke, L.; North, K. E.; Kraft, P.; Morrison, A. C.; Esko, T.; Wilson, J. F. GWAS for Male-Pattern Baldness Identifies 71 Susceptibility Loci Explaining 38% of the Risk. *Nat. Commun.* **2017**, *8*, 1584.

(3) Unger, W. P.; Unger, R. H. Hair Transplanting: An Important but Often Forgotten Treatment for Female Pattern Hair Loss. *J. Am. Acad. Dermatol.* **2003**, *49*, 853−860.

(4) Matilainen, V.; Laakso, M.; Hirsso, P.; Koskela, P.; Rajala, U.; Keinanen-Kiukaanniemi, S. Hair Loss, Insulin Resistance, and Heredity in Middle-Aged Women. a Population-Based Study. *Eur. J. Cardiovasc. Prev. Rehabil.* **2003**, *10*, 227−231.

(5) Garcia-Hernandez, M. J.; Ruiz-Doblado, S.; Rodriguez-Pichardo, A.; Camacho, F. Alopecia Areata, Stress and Psychiatric Disorders: A Review. *J. Dermatol.* **1999**, *26*, 625−632.

(6) Tajima, M.; Hamada, C.; Arai, T.; Miyazawa, M.; Shibata, R.; Ishino, A. Characteristic Features of Japanese Women's Hair with Aging and with Progressing Hair Loss. *J. Dermatol. Sci.* **2007**, *45*, 93−103.

(7) Roberts, J. L.; Fiedler, V.; Imperato-McGinley, J.; Whiting, D.; Olsen, E.; Shupack, J.; Stough, D.; DeVillez, R.; Rietschel, R.; Savin, R.; Bergfeld, W.; Swinehart, J.; Funicella, T.; Hordinsky, M.; Lowe, N.; Katz, I.; Lucky, A.; Drake, L.; Price, V. H.; Weiss, D.; et al. Clinical Dose Ranging Studies with Finasteride, a Type 2 5α-Reductase Inhibitor, in Men with Male Pattern Hair Loss. *J. Am. Acad. Dermatol.* **1999**, *41*, 555−563.

(8) Leyden, J.; Dunlap, F.; Miller, B.; Winters, P.; Lebwohl, M.; Hecker, D.; Kraus, S.; Baldwin, H.; Shalita, A.; Draelos, Z.; Markou, M.; Thiboutot, D.; Rapaport, M.; Kang, S.; Kelly, T.; Pariser, D.; Webster, G.; Hordinsky, M.; Rietschel, R.; Katz, H. I.; et al. Finasteride in the Treatment of Men with Frontal Male Pattern Hair Loss. *J. Am. Acad. Dermatol.* **1999**, *40*, 930−937.

(9) Olsen, E. A.; Messenger, A. G.; Shapiro, J.; Bergfeld, W. F.; Hordinsky, M. K.; Roberts, J. L.; Stough, D.; Washenik, K.; Whiting, D. A. Evaluation and Treatment of Male and Female Pattern Hair Loss. *J. Am. Acad. Dermatol.* **2005**, *52*, 301−311.

(10) Asakawa, M.; Yoshioka, T.; Matsutani, T.; Hikita, I.; Suzuki, M.; Oshima, I.; Tsukahara, K.; Arimura, A.; Horikawa, T.; Hirasawa, T.; Sakata, T. Association of a Mutation in TRPV3 with Defective Hair Growth in Rodents. *J. Invest. Dermatol.* **2006**, *126*, 2664−2672.

(11) Sinclair, R.; Asgari, A. Male Pattern Androgenetic Alopecia. *Med. Today* **2011**, *12*, 71−73.

(12) Olsen, E. A.; Dunlap, F. E.; Funicella, T.; Koperski, J. A.; Swinehart, J. M.; Tschen, E. H.; Trancik, R. J. A Randomized Clinical Trial of 5% Topical Minoxidil *versus* 2% Topical Minoxidil and Placebo in the Treatment of Androgenetic Alopecia in Men. *J. Am. Acad. Dermatol.* **2002**, *47*, 377−385.

(13) Anderson, R. R. Lasers in Dermatology–a Critical Update. *J. Dermatol.* **2000**, *27*, 700−705.

DOI: 10.1021/acsnano.8b05568
ACS Nano 2018, 12, 9587−9595

(14) Avci, P.; Gupta, G. K.; Clark, J.; Wikonkal, N.; Hamblin, M. R. Low-Level Laser (Light) Therapy (LLLT) for Treatment of Hair Loss. *Lasers Surg. Med.* **2014**, *46*, 144−151.
(15) Lanzafame, R. J.; Blanche, R. R.; Bodian, A. B.; Chiacchierini, R. P.; Fernandez-Obregon, A.; Kazmirek, E. R. The Growth of Human Scalp Hair Mediated by Visible Red Light Laser and LED Sources in Males. *Lasers Surg. Med.* **2013**, *45*, 487−495.
(16) Yoon, S. Y.; Yoon, J. S.; Jo, S. J.; Shin, C. Y.; Shin, J. Y.; Kim, J. Il; Kwon, O.; Kim, K. H. A Role of Placental Growth Factor in Hair Growth. *J. Dermatol. Sci.* **2014**, *74*, 125−134.
(17) Kim, W.-S.; Calderhead, R. G. Is Light-Emitting Diode Phototherapy (LED-LLLT) Really Effective? *Laser Ther.* **2011**, *20*, 205−215.
(18) Avci, P.; Gupta, A.; Sadasivam, M.; Vecchio, D.; Pam, Z.; Pam, N.; Hamblin, M. R. Low-Level Laser (Light) Therapy (LLLT) in Skin: Stimulating, Healing, Restoring. *Semin. Cutan. Med. Surg.* **2013**, *32*, 41−52.
(19) Dong, Y.; Zhou, G.; Chen, J.; Shen, L.; Jianxin, Z.; Xu, Q.; Zhu, Y. A New LED Device Used for Photodynamic Therapy in Treatment of Moderate to Severe Acne Vulgaris. *Photodiagn. Photodyn. Ther.* **2016**, *13*, 188−195.
(20) Kim, T.-H.; Kim, N.-J.; Youn, J.-I. Evaluation of Wavelength-Dependent Hair Growth Effects on Low-Level Laser Therapy: An Experimental Animal Study. *Lasers Med. Sci.* **2015**, *30*, 1703−1709.
(21) Fushimi, T.; Inui, S.; Ogasawara, M.; Nakajima, T.; Hosokawa, K.; Itami, S. Narrow-Band Red LED Light Promotes Mouse Hair Growth through Paracrine Growth Factors from Dermal Papilla. *J. Dermatol. Sci.* **2011**, *64*, 246−248.
(22) Nelson, E. C.; Dias, N. L.; Bassett, K. P.; Dunham, S. N.; Verma, V.; Miyake, M.; Wiltzius, P.; Rogers, J. A.; Coleman, J. J.; Li, X.; Braun, P. V. Epitaxial Growth of Three-Dimensionally Architectured Optoelectronic Devices. *Nat. Mater.* **2011**, *10*, 676−681.
(23) Lee, K. J.; Koo; Park. Biointegrated Flexible Inorganic Light Emitting Diodes. *Nanobiosensors Dis. Diagnosis* **2012**, 5.
(24) Grossman, M. C.; Dierickx, C.; Farinelli, W.; Flotte, T.; Anderson, R. R. Damage to Hair Follicles by Normal-Mode Ruby Laser Pulses. *J. Am. Acad. Dermatol.* **1996**, *35*, 889−894.
(25) Lin, T.-Y. D.; Manuskiatti, W.; Dierickx, C. C.; Farinelli, W. A.; Fisher, M. E.; Flotte, T.; Baden, H. P.; Anderson, R. R. Hair Growth Cycle Affects Hair Follicle Destruction by Ruby Laser Pulses. *J. Invest. Dermatol.* **1998**, *111*, 107−113.
(26) Bäumler, W.; Scherer, K.; Abels, C.; Neff, S.; Landthaler, M.; Szeimies, R. M. The Effect of Different Spot Sizes on the Efficacy of Hair Removal Using a Long-Pulsed Diode Laser. *Dermatol. Surg.* **2002**, *28*, 118−121.
(27) Chung, H.; Dai, T.; Sharma, S. K.; Huang, Y.-Y.; Carroll, J. D.; Hamblin, M. R. The Nuts and Bolts of Low-Level Laser (Light) Therapy. *Ann. Biomed. Eng.* **2012**, *40*, 516−533.
(28) Park, S.-I.; Xiong, Y.; Kim, R.-H.; Elvikis, P.; Meitl, M.; Kim, D.-H.; Wu, J.; Yoon, J.; Yu, C.-J.; Liu, Z.; Huang, Y.; Hwang, K.-C.; Ferreira, P.; Li, X.; Choquette, K.; Rogers, J. A. Printed Assemblies of Inorganic Light-Emitting Diodes for Deformable and Semitransparent Displays. *Science* **2009**, *325*, 977−981.
(29) Lee, S. Y.; Park, K.-I.; Huh, C.; Koo, M.; Yoo, H. G.; Kim, S.; Ah, C. S.; Sung, G. Y.; Lee, K. J. Water-Resistant Flexible GaN LED on a Liquid Crystal Polymer Substrate for Implantable Biomedical Applications. *Nano Energy* **2012**, *1*, 145−151.
(30) Kim, T. -i.; McCall, J. G.; Jung, Y. H.; Huang, X.; Siuda, E. R.; Li, Y.; Song, J.; Song, Y. M.; Pao, H. A.; Kim, R.-H.; Lu, C.; Lee, S. D.; Song, I. − S.; Shin, G.; Al-Hasani, R.; Kim, S.; Tan, M. P.; Huang, Y.; Omenetto, F. G.; Rogers, J. A.; et al. Injectable, Cellular-Scale Optoelectronics with Applications for Wireless Optogenetics. *Science* **2013**, *340*, 211−216.
(31) Park, S. Il; Brenner, D. S.; Shin, G.; Morgan, C. D.; Copits, B. A.; Chung, H. U.; Pullen, M. Y.; Noh, K. N.; Davidson, S.; Oh, S. J.; Yoon, J.; Jang, K. − I.; Samineni, V. K.; Norman, M.; Grajales-Reyes, J. G.; Vogt, S. K.; Sundaram, S. S.; Wilson, K. M.; Ha, J. S.; Xu, R.; et al. Soft, Stretchable, Fully Implantable Miniaturized Optoelectronic Systems for Wireless Optogenetics. *Nat. Biotechnol.* **2015**, *33*, 1280−1286.
(32) Lee, S. H.; Kim, J.; Shin, J. H.; Lee, H. E.; Kang, I. S.; Gwak, K.; Kim, D. S.; Kim, D.; Lee, K. J. Optogenetic Control of Body Movements *via* Flexible Vertical Light-Emitting Diodes on Brain Surface. *Nano Energy* **2018**, *44*, 447−455.
(33) Lee, H. E.; Kim, S.; Ko, J.; Yeom, H.; Byun, C.; Lee, S. H.; Joe, D. J.; Im, T.; Park, S. K.; Lee, K. J. Skin-Like Oxide Thin-Film Transistors for Transparent Displays. *Adv. Funct. Mater.* **2016**, *26*, 6170−6178.
(34) Park, S.-I.; Le, A.-P.; Wu, J.; Huang, Y.; Li, X.; Rogers, J. A. Light Emission Characteristics and Mechanics of Foldable Inorganic Light-Emitting Diodes. *Adv. Mater.* **2010**, *22*, 3062−3066.
(35) Lee, J. M.; Choung, J. W.; Yi, J.; Lee, D. H.; Samal, M.; Yi, D. K.; Lee, C. H.; Yi, G. C.; Paik, U.; Rogers, J. A.; Park, W. I. Vertical Pillar-Superlattice Array and Graphene Hybrid Light Emitting Diodes. *Nano Lett.* **2010**, *10*, 2783−2788.
(36) Kim, R. H.; Kim, D. H.; Xiao, J.; Kim, B. H.; Park, S. Il; Panilaitis, B.; Ghaffari, R.; Yao, J.; Li, M.; Liu, Z.; Malyarchuk, V.; Kim, D. G.; Le, A. − P.; Nuzzo, R. G.; Kaplan, D. L.; Omenetto, F. G.; Huang, Y.; Kang, Z.; Rogers, J. A. Waterproof AlInGaP Optoelectronics on Stretchable Substrates with Applications in Biomedicine and Robotics. *Nat. Mater.* **2010**, *9*, 929−937.
(37) Kim, R.-H.; Bae, M.; Kim, D. G.; Cheng, H.; Kim, B. H.; Kim, D.-H.; Li, M.; Wu, J.; Du, F.; Kim, H.-S.; Kim, S.; Estrada, D.; Hong, S. W.; Huang, Y.; Pop, E.; Rogers, J. A. Stretchable, Transparent Graphene Interconnects for Arrays of Microscale Inorganic Light Emitting Diodes on Rubber Substrates. *Nano Lett.* **2011**, *11*, 3881−3886.
(38) Kim, R. H.; Tao, H.; Kim, T. Il; Zhang, Y.; Kim, S.; Panilaitis, B.; Yang, M.; Kim, D. H.; Jung, Y. H.; Kim, B. H.; Li, Y.; Huang, Y.; Omenetto, F. G.; Rogers, J. A. Materials and Designs for Wirelessly Powered Implantable Light-Emitting Systems. *Small* **2012**, *8*, 2812−2818.
(39) Jeong, C. K.; Park, K.-I.; Son, J. H.; Hwang, G.-T.; Lee, S. H.; Park, D. Y.; Lee, H. E.; Lee, H. K.; Byun, M.; Lee, K. J. Self-Powered Fully-Flexible Light-Emitting System Enabled by Flexible Energy Harvester. *Energy Environ. Sci.* **2014**, *7*, 4035−4043.
(40) Lee, H. E.; Choi, J.; Lee, S. H.; Jeong, M.; Shin, J. H.; Joe, D. J.; Kim, D.; Kim, C. W.; Park, J. H.; Lee, J. H.; Kim, D.; Shin, C. − S.; Lee, K. J. Monolithic Flexible Vertical GaN Light-Emitting Diodes for a Transparent Wireless Brain Optical Stimulator. *Adv. Mater.* **2018**, *30*, 1800649.
(41) Lee, H. E.; Park, J. H.; Kim, T. J.; Im, D.; Shin, J. H.; Kim, D. H.; Mohammad, B.; Kang, I.-S.; Lee, K. J. Novel Electronics for Flexible and Neuromorphic Computing. *Adv. Funct. Mater.* **2018**, *28*, 1801690.
(42) Jagdeo, J.; Austin, E.; Mamalis, A.; Wong, C.; Ho, D.; Siegel, D. M. Light-Emitting Diodes in Dermatology: A Systematic Review of Randomized Controlled Trials. *Lasers Surg. Med.* **2018**, *50*, 613−628.
(43) Lanzafame, R. J.; Blanche, R. R.; Chiacchierini, R. P.; Kazmirek, E. R.; Sklar, J. A. The Growth of Human Scalp Hair in Females Using Visible Red Light Laser and LED Sources. *Lasers Surg. Med.* **2014**, *46*, 601−607.
(44) Kim, T.; Hyun Lee, S.; Li, Y.; Shi, Y.; Shin, G.; Dan Lee, S.; Huang, Y.; Rogers, J. a.; Su Yu, J. Temperature- and Size-Dependent Characteristics in Ultrathin Inorganic Light-Emitting Diodes Assembled by Transfer Printing. *Appl. Phys. Lett.* **2014**, *104*, No. 051901.
(45) Gong, Z.; Jin, S.; Chen, Y.; McKendry, J.; Massoubre, D.; Watson, I. M.; Gu, E.; Dawson, M. D. Size-Dependent Light Output, Spectral Shift, and Self-Heating of 400 Nm InGaN Light-Emitting Diodes. *J. Appl. Phys.* **2010**, *107*, No. 013103.
(46) Chen-Fu Chu; Chao-Chen Cheng; Wen-Huan Liu; Jiunn-Yi Chu; Feng-Hsu Fan; Hao-Chun Cheng; Trung Doan; Chuong Anh Tran. High Brightness GaN Vertical Light-Emitting Diodes on Metal Alloy for General Lighting Application. *Proc. IEEE* **2010**, *98*, 1197−1207.

DOI: 10.1021/acsnano.8b05568
ACS Nano 2018, 12, 9587−9595

(47) Güngörmüş, M.; Akyol, U. The Effect of Gallium-Aluminum-Arsenide 808-Nm Low-Level Laser Therapy on Healing of Skin Incisions Made Using a Diode Laser. *Photomed. Laser Surg.* **2009**, *27*, 895−899.

(48) Yoo, H. G.; Byun, M.; Jeong, C. K.; Lee, K. J. Performance Enhancement of Electronic and Energy Devices *via* Block Copolymer Self-Assembly. *Adv. Mater.* **2015**, *27*, 3982−3998.

(49) Grandinétti, V. d. S.; Miranda, E. F.; Johnson, D. S.; de Paiva, P. R. V.; Tomazoni, S. S.; Vanin, A. A.; Albuquerque-Pontes, G. M.; Frigo, L.; Marcos, R. L.; de Carvalho, P. de T. C.; Leal-Junior, E. C. P. The Thermal Impact of Phototherapy with Concurrent Super-Pulsed Lasers and Red and Infrared LEDs on Human Skin. *Lasers Med. Sci.* **2015**, *30*, 1575−1581.

(50) Li, Y.; Shi, Y.; Song, J.; Lu, C.; Kim, T. Il; Rogers, J. A.; Huang, Y. Thermal Properties of Microscale Inorganic Light-Emitting Diodes in a Pulsed Operation. *J. Appl. Phys.* **2013**, *113*, 144505.

(51) Hashmi, J. T.; Huang, Y. Y.; Sharma, S. K.; Kurup, D. B.; De Taboada, L.; Carroll, J. D.; Hamblin, M. R. Effect of Pulsing in Low-Level Light Therapy. *Lasers Surg. Med.* **2010**, *42*, 450−466.

(52) Zhang, H. X.; Massoubre, D.; McKendry, J.; Gong, Z.; Guilhabert, B.; Griffin, C.; Gu, E.; Jessop, P. E.; Girkin, J. M.; Dawson, M. D. Individually-Addressable Flip-Chip AlInGaN Micropixelated Light Emitting Diode Arrays with High Continuous and Nanosecond Output Power. *Opt. Express* **2008**, *16*, 9918.

(53) Webb, R. C.; Bonifas, A. P.; Behnaz, A.; Zhang, Y.; Yu, K. J.; Cheng, H.; Shi, M.; Bian, Z.; Liu, Z.; Kim, Y.-S.; Yeo, W. − H.; Park, J. S.; Song, J.; Li, Y.; Huang, Y.; Gorbach, A. M.; Rogers, J. A. Ultrathin Conformal Devices for Precise and Continuous Thermal Characterization of Human Skin. *Nat. Mater.* **2013**, *12*, 938−944.

(54) Merano, M.; Aiello, A.; Van Exter, M. P.; Woerdman, J. P. Observing Angular Deviations in the Specular Reflection of a Light Beam. *Nat. Photonics* **2009**, *3*, 337−340.

(55) Akahane, Y.; Asano, T.; Song, B.; Noda, S. High- Q Photonic Nanocavity in a Two-Dimensional Photonic Crystal. *Nature* **2003**, *425*, 944.

(56) Kim, D.-H.; Ahn, J.-H.; Choi, W. M.; Kim, H.-S.; Kim, T.-H.; Song, J.; Huang, Y. Y.; Liu, Z.; Lu, C.; Rogers, J. A. Stretchable and Foldable Silicon Integrated Circuits. *Science* **2008**, *320*, 507−511.

(57) Kaltenbrunner, M.; Sekitani, T.; Reeder, J.; Yokota, T.; Kuribara, K.; Tokuhara, T.; Drack, M.; Schwödiauer, R.; Graz, I.; Bauer-Gogonea, S.; Bauer, S.; Someya, T. An Ultra-Lightweight Design for Imperceptible Plastic Electronics. *Nature* **2013**, *499*, 458−463.

(58) Kim, D.-H.; Lu, N.; Ma, R.; Kim, Y.-S.; Kim, R.-H.; Wang, S.; Wu, J.; Won, S. M.; Tao, H.; Islam, A.; Yu, K. J.; Kim, T. − I.; Chowdhury, R.; Ying, M.; Xu, L.; Li, M.; Chung, H. − J.; Keum, H.; McCormick, M.; Liu, P.; et al. Epidermal Electronics. *Science* **2011**, *333*, 838−843.

(59) Sheen, Y. S.; Fan, S. M. Y.; Chan, C. C.; Wu, Y. F.; Jee, S. H.; Lin, S. J. Visible Red Light Enhances Physiological Anagen Entry *in Vivo* and Has Direct and Indirect Stimulative Effects *in Vitro*. *Lasers Surg. Med.* **2015**, *47*, 50−59.

(60) Millar, S. E.; et al. WNT Signaling in the Control of Hair Growth and Structure. *Dev. Biol.* **1999**, *207*, 133−149.

(61) Noramly, S.; Freeman, A.; Morgan, B. A. Beta-Catenin Signaling Can Initiate Feather Bud Development. *Development* **1999**, *126*, 3509−3521.

(62) Widelitz, R. B.; Jiang, T. X.; Lu, J.; Chuong, C. M. β-Catenin in Epithelial Morphogenesis: Conversion of Part of Avian Foot Scales into Feather Buds with a Mutated β-Catenin. *Dev. Biol.* **2000**, *219*, 98−114.

(63) Huelsken, J.; Vogel, R.; Erdmann, B.; Cotsarelis, G.; Birchmeier, W. β-Catenin Controls Hair Follicle Morphogenesis and Stem Cell Differentiation in the Skin. *Cell* **2001**, *105*, 533−545.

(64) Choi, Y. S.; Zhang, Y.; Xu, M.; Yang, Y.; Ito, M.; Peng, T.; Cui, Z.; Nagy, A.; Hadjantonakis, A. K.; Lang, R. A.; Cotsarelis, G.; Andl, T.; Morrisey, E. E.; Millar, S. E. Distinct Functions for Wnt/β-Catenin in Hair Follicle Stem Cell Proliferation and Survival and Interfollicular Epidermal Homeostasis. *Cell Stem Cell* **2013**, *13*, 720−733.

(65) Park, J. H.; Hwang, G. T.; Kim, S.; Seo, J.; Park, H. J.; Yu, K.; Kim, T. S.; Lee, K. J. Flash-Induced Self-Limited Plasmonic Welding of Silver Nanowire Network for Transparent Flexible Energy Harvester. *Adv. Mater.* **2017**, *29*, 1603473.

(66) Hwang, G. T.; Annapureddy, V.; Han, J. H.; Joe, D. J.; Baek, C.; Park, D. Y.; Kim, D. H.; Park, J. H.; Jeong, C. K.; Park, K. Il; Choi, J. − J.; Kim, D. K.; Ryu, J.; Lee, K. J. Self-Powered Wireless Sensor Node Enabled by an Aerosol-Deposited PZT Flexible Energy Harvester. *Adv. Energy Mater.* **2016**, *6*, 1600237.

DOI: 10.1021/acsnano.8b05568
ACS Nano 2018, 12, 9587−9595